Supporting Information

Synergistic Effect of Doped Nitrogen and Oxygen-containing Functional Groups for Electrochemical Synthesis of Hydrogen Peroxide

Zhikang Bao†, Jinyan Zhao†, Shijie Zhang, Lei Ding, Xiaoge Peng, Guoliang Wang, Zijiang Zhao, Xing Zhong, Zihao Yao, Jianguo Wang**

Institute of Industrial Catalysis, College of Chemical Engineering, State Key Laboratory Breeding Base of Green-Chemical Synthesis Technology, Zhejiang University of Technology, Hangzhou 310032 China.

†Z.K. Bao and J.Y. Zhao contribute to this work equally

*Correspondence and requests for materials should be addressed to Z.H.Y. (email: yaozihao@zjut.edu.cn) and J.G.W. (email: jgw@zjut.edu.cn).

Contents:

Supporting experimental methods

1. Materials Synthesis.

1.1 Chemicals and materials

In terms of raw materials, in addition to Xylan ($C_5H_{10}O_5$), which is a product of Beijing Huawei Ruike Chemical Co., Ltd., Melamine ($C_3H_6N_6$), α-Cellulose (65 μm), Glucose ($C_6H_{12}O_6$) and Fructose ($C_6H_{12}O_6$) are all purchased from Shanghai Macklin Inc Co., Ltd. In terms of electrolyte, potassium hydroxide (KOH) and anhydrous sodium sulfate (Na_2SO_4) were also purchased from Shanghai Macklin Inc Co., Ltd., and sulfuric acid (H_2SO_4) was from Shanghai Lingfeng Chemical Reagent Co., Ltd. Deionized (DI) water was used in all experiments, which was made by the laboratory. All of the reagents were of analytical grade (AR), and used without further purification.

1.2 Synthesis of N-CBMC-XX

In a typical synthesis, using the similar as chemical vapor deposition (CVD) method, 1.0 g of melamine and 1.0 g of α-cellulose are placed in two porcelain boats. In particular, the two porcelain boats containing raw materials are covered to prevent excessive loss during the pyrolysis process. After that, the two porcelain boats were put together in a tube furnace, and the temperature was raised to 500°C at a rate of 5°C/min under a nitrogen atmosphere. The high temperature was maintained for 3 hours for pyrolysis. After it was naturally cooled, the porcelain at the downwind was taken out, and the resulting pyrolysis was ground. The product is then prepared nitrogen-doped cellulose-based mesoporous carbon material (N-CBMC-500) catalyst. It is worth noting that melamine was placed on the upper air inlet, and α-cellulose was placed on the lower air outlet.

The catalyst products at different pyrolysis temperatures were also prepared here. For example, except that the pyrolysis temperature was changed to 400 °C, the samples obtained without other preparation conditions were named N-CBMC-400. The pyrolysis temperature of 600 ℃ and 700 ℃ are also named in the same way (N-CBMC-600 and N-CBMC-700).

Synthesis of N-XBMC-500, N-GBMC-500 and N-FBMC-500

Similarly, the preparation methods of N-XBMC-500, N-GBMC-500 and N-FBMC-500 are similar to N-CBMC-500, except that the raw materials are Xylan, Glucose and Fructose, respectively.

Synthesis of CBMC-500, XBMC-500, GBMC-500 and FBMC-500

For comparison, a material without melamine was prepared and denoted as CBMC-500 (XBMC-500, GBMC-500 and FBMC-500). Precisely, 1.0 g of α-cellulose (Xylan, Glucose and Fructose) was placed in a porcelain boat for use. The porcelain boat with α-cellulose was pyrolyzed under a flowing N_2 atmosphere in a tube furnace. The ramping program was the same as N-CBMC-500.

2. Materials characterization

The scanning electron microscope (SEM) equipment is Phenom ProX with field emission. The transmission electron microscope (TEM, Tecnai G2F30S-Twin) is operated at 300 kV. The test procedure is: Disperse the sample on a carbon-coated copper net, dry it under infrared light, and observe it directly. Use STEM (FEI Titan G2 80-200 ChemiSTEM) to observe the energy dispersive X-ray spectrum (EDX). X-ray powder diffraction (XRD) was performed on an X-ray diffractometer (PANalytical X-pert Pro) with Cu Ka irradiation (λ = 1.5418 Å) at 40 kV and 40 mA. The sample's X-ray photoelectron spectroscopy (XPS) is tested by X-ray photoelectron spectroscopy (Thermo Scientific K-Alpha). The absorption spectrum was recorded using an ultraviolet-visible spectrophotometer (Shanghai Mapada P4), and FTIR was performed in Nicolet iS50. The American ASAP2460 analyzer is used to measure Brunauer-Emmett-Teller (BET) specific surface area and pore size distribution. Elemental analysis (EA) measurement uses the Elementar Vario EL cubes instrument.

3. Electrochemical Details.

Electrochemical Instrument

All electrochemical performance tests are carried out on the electrochemical workstation (CHI 760, Shanghai Chenhua Instrument Co., Ltd.), including the selective performance test and yield test of the electrocatalytic oxygen reduction reaction to generate hydrogen peroxide. The same uses the traditional three-electrode system: the working electrode (WE) is a drop-cast electrode, the counter electrode (CE) is a

platinum wire or stable anode (MMO), and the saturated calomel electrode (SCE) is used as the reference electrode (RE).

To evaluate the selectivity of the catalyst and the number of electrons transferred, a rotating ring disk electrode (RRDE-3A, ALS Co., Ltd) device was used, including a glassy carbon (GC) disk (diameter 4 mm) surrounded by a Pt ring (inner diameter 5 mm, outer diameter 7 mm) electrode. Before use, the electrode was polished on elk leather (PK-3, ALS Co., Ltd) with a uniformly dispersed 0.05μm alumina suspension (Gaoss Union, Inc.), then washed with pure water ultrasonically and under ambient conditions.

Electrode Preparation

For RRDE (selectivity and transfer number): To prepare working electrodes of drop-casted N-CBMC-500, the same amount (~4 mg) of N-CBMC-500 powders was suspended in the 1:9 (v/v) mixture (Total volume was 1mL) of Nafion solution (DuPont D520, 5 wt%) and absolute ethanol by sonicating for 60 min. The obtained solution was called catalysts "ink". Then, 5.0 μL of homogeneous "ink" was slowly dispersed on the GC area of RRDE electrode and then dried under infrared light.

For Flow Cell (yield): To evaluate the output (yield) of hydrogen peroxide, the method adopted by the working electrode: spray the catalyst dispersion containing a certain amount of nafion solution directly on the diffusion layer (Suzhou Shengernuo, YLS-30T), and use the whole as a working electrode, The purpose is to obtain more siginificant current. The effective area of this experimental device (Flow cell, Figure S1) is 3 × 3cm. Use scissors to cut the diffusion layer into small pieces of 3 cm × 3 cm as the working area, and spray the catalyst dispersion on the diffusion layer to obtain the corresponding cathode electrode. The anode electrode directly uses commercially available stable metal oxide anode materials (MMO, $IrO_2Ta_2O_5$-Ti).

Electrochemical Measurements

To better compare potentials, all the reported potentials were referred to as the reversible hydrogen electrode (RHE) potential, according to pH values of O_2-saturated electrolytes.

$$E(RHE) = E(SCE) + 0.0591 \times pH + 0.241V$$

Unless otherwise specified, the E mentioned in this article were relative to the RHE.

For RRDE: First, the electrochemical oxygen reduction reaction occurs in a single electrolytic cell with 60 mL of electrolyte (0.1 M KOH). Before the measurement, let in O_2 gas at a flow rate of 30 sccm for at least 30 min, to make the electrolyte saturated with oxygen. During the measurement process, O_2 remains unchanged, and the oxygen concentration in the electrolyte is always at the maximum.

Next, for the two-electron oxygen reduction reaction ($2e^-$ ORR), connect the CHI 760 electrochemical workstation and RRDE to test the performance. The catalyst-coated RRDE electrode is equipped as a working electrode on the RRDE, connected to the counter electrode and the reference electrode. The electrochemical workstation performs cyclic voltammetry (CV) and linear sweep voltammetry (LSV) tests, respectively. The CV test voltage range is 0 V-1.20 V, the scan rate is 50 mV/s, and the loop voltage is turned off. The LSV test voltage range is 1.20-0 V, and the scan rate is 10 mV/s. At this time, the ring voltage is set to a constant value of 1.5 V. In addition, LSV tests at different speeds (rpm) were performed to characterize its kinetics. For comparison, use Ar instead of O_2 to pass the electrolyte into the CV test for contrast (Figure 3a). The H_2O_2 selectivity (%) and the electron transfer number (n) was calculated based on the current of both disk and ring electrodes (Equation (1)). And the corresponding electron transfer number (n) can also be obtained by Equation 2.

$$H_2O_2\% = 200 \times \frac{I_R/N}{I_D + I_R/N} \quad (1)$$

$$n = 4 \times \frac{I_D/N}{I_D + I_R/N} \quad (2)$$

where I_R is the ring current, I_D is the disk current, and N is the collection efficiency.

At different rotation rates, the collection efficiency was also calibrated in 0.1 M KOH + 10 mM $K_3Fe(CN)_6$ electrolyte.[1, 2] As a result, the measured collection efficiency was 40% in Figure S2. Detailed measure for N were described in the next text.

The principle of the RRDE to test the selectivity of H_2O_2 is that the H_2O_2 generated

at the disk electrode migrates to the concentric platinum ring electrode by rotating motion and then is oxidized back to H_2O and O_2 on the ring electrode. And the Faradaic efficiency[3] can be obtained by:

$$Faradaic\ efficiency(\%) = \frac{\frac{I_{ring}}{N}}{I_{disk}} \times 100$$

The electrochemical impedance spectroscopy (EIS) was conducted at 1.1 V vs. RHE from 345500 to 10 Hz to determine the uncompensated resistance (Ru) in a high-frequency range for iR-correction.

For Flow Cell: The H_2O_2 production (yield) performance was tested in a self-made electrolytic cell (Flow cell) using the constant current method at each fixed potential for 60 minutes. In the flow cell, cut NEPEM-115 membrane (Jiangsu Kerun Membrane Material Co., Ltd.) or FAB-PK-130 (fumasep) into small pieces (4 cm × 4 cm) to separate the anolyte and catholyte, and the anode and cathode chambers. The chamber uses a peristaltic pump to circulate 0.1 M KOH (0.5 M Na_2SO_4, 0.5M H_2SO_4) electrolyte at a flow rate of 30 mL min^{-1}. And the working electrode of the device is composed of catalyst and diffusion layer sprayed with different loadings (0.1 mg/cm^2~ 0.5 mg/cm^2).

During the operation of the equipment, O_2 was fed into the flow channel pool at a rate of 30 mL min^{-1} and diffused into the catalyst layer from the back of the hydrophobic diffusion layer. After constant voltage electrolysis for a certain time (60 min), it is necessary to test the concentration of H_2O_2 produced. We use the classic potassium titanate oxalate color method.[4] The basis of this method is the formation of titanium (IV)-peroxide complex in the presence of sulfuric acid. The detailed process of this method could be described as follows: a certain volume (1 mL) of the sample to be measured was added into the as-prepared potassium titanium oxalate $K_2TiO(C_2O_4)_2$ solution (0.5 M, 1 mL) and 3 M H_2SO_4 solution (1 mL), and then the colour of the solution changes into yellow because of the above chromogenic reaction. Next, the UV-vis technology (at 400 nm) was used to determine and calculate the content of the H_2O_2 in the samples (The corresponding standard curve is in Figure S3).

The following equations can describe the relationships of Faradaic efficiency in

Flow cell setup:

$$Faradaic\ efficiency\ (\%) = 100 \times \frac{2 \times C \times V \times F}{Q}$$

where C is the produced H_2O_2 concentration (mol L^{-1}), V is the volume of electrolyte (L), F is the faraday constant (96485 C mol^{-1}), Q is the passed charge amount (C).

Measuring the Collection Efficiency of RRDE.

The collection efficiency (N) was measured on a blank RRDE (0.1256 cm^2 GC disc area, 0.1884 cm^2 Pt ring area) electrode. The principle is to use the single-electron reaction of the reversible redox-ferrocyanide/ferricyanide system to determine the collection efficiency (N) of the Pt ring.[1] Specifically, 0.1 M KOH with a concentration of 10 mM potassium ferricyanide (III) ($K_3[Fe(CN)_6]$, Macklin, 99%) is used as the electrolyte. Before the test, the electrolyte is ventilated with Ar gas for more than 30 minutes to eliminate dissolved oxygen's influence on the test. In addition, Ar gas was kept flowing during the measurement. The test procedure is the standard LSV method.

RRDE voltammograms were recorded by performing LSV on the disk from 1.2 V to 0 V vs. RHE at 10 mV/s and different rotation rates (400, 625, 900, 1225, 1600 and 2025 rpm). Meanwhile the ring was held at 1.50 V vs. RHE (Figure S2a). The collection efficiency (N) of RRDE is calculated using the equation:

$$N = I_{ring}/I_{disk}$$

where I_{ring} and I_{disk} are the ring and the disk current, respectively. The ferricyanide reduced on the disk electrode is sent to the Pt ring range due to diffusion, so the voltage applied on the Pt ring will reduce the ferrocyanide to ferricyanide. The current generated is a reflection of the collection efficiency that a platinum ring can provide. When both ferricyanide reduction on the bare GC disk and ferrocyanide oxidation on the Pt ring became diffusion-limited,[5] the collection efficiency was found to be 0.40 and was independent of the RRDE rotation rate (Figure S2b)

4. Calculation Methods

In this work, all the simulations were carried out for the selective hydrogenation of acetylene within the framework of the generalized gradient approximation with the Perdew-Burke- Ernzerh [6] of functional in the VASP code.[7, 8] All the calculations were

calculated by DFT-D3 method, including van der Waals interactions.[9-11] The PAW was carried out to describe the interaction between core-electron and valence electron. The cutoff energy of plane-wave basis expansion was set to 400 eV. Electronic convergence was set to 10^{-5} eV, and geometries were converged to less than 0.05 eV/Å. The structure optimization was calculated using the conjugate-gradient algorithm. A (7 × 7) graphene surface unit cell with the lattice constants A = 14.76 Å, B = 14.76 Å, and C = 21 Å was built, and 2 × 2 × 1 Monkhorst−Pack k-point mesh sampling was used.[12] All surfaces were built using periodic slabs of one layer.

II Supplementary Results

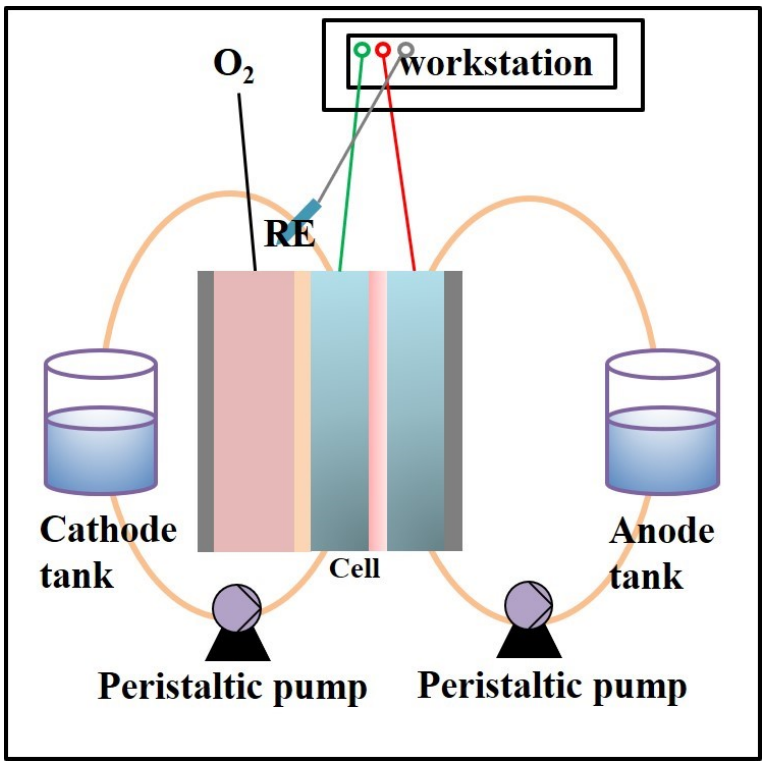

Figure S1. Schematic diagram of the overall equipment for electrochemical selective oxygen reduction to produce H_2O_2.

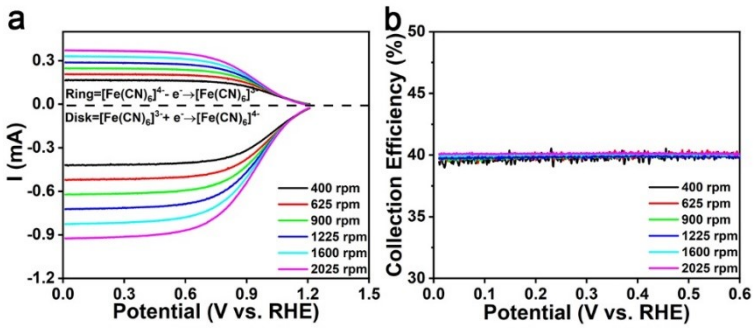

Figure S2. Measure of the collection efficiency of the blank RRDE in Ar-saturated 0.1 M KOH dissolved with 10 mM of $K_3[Fe(CN)_6]$. (a) RRDE voltammograms recorded at different rotation rates by performing LSV on the disk from 1.2 V to 0 V vs. RHE at 50 mV/s while holding the ring at 1.50 V vs. RHE, (b) the corresponding collection efficiency of RRDE voltammograms as a function of the potential. All potentials in this figure are presented without iR-correction.

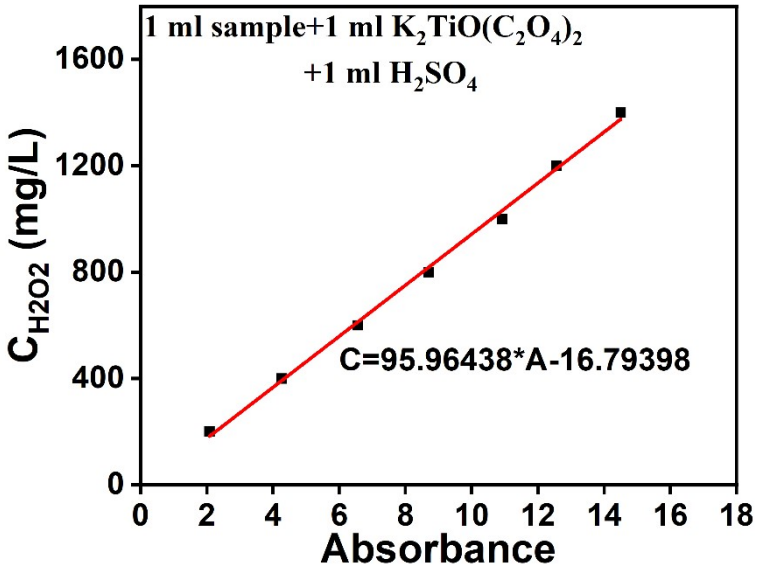

Figure S3. The calibration curve of $K_2TiO(C_2O_4)_2$ solution and the standard curve of its reaction with hydrogen peroxide..

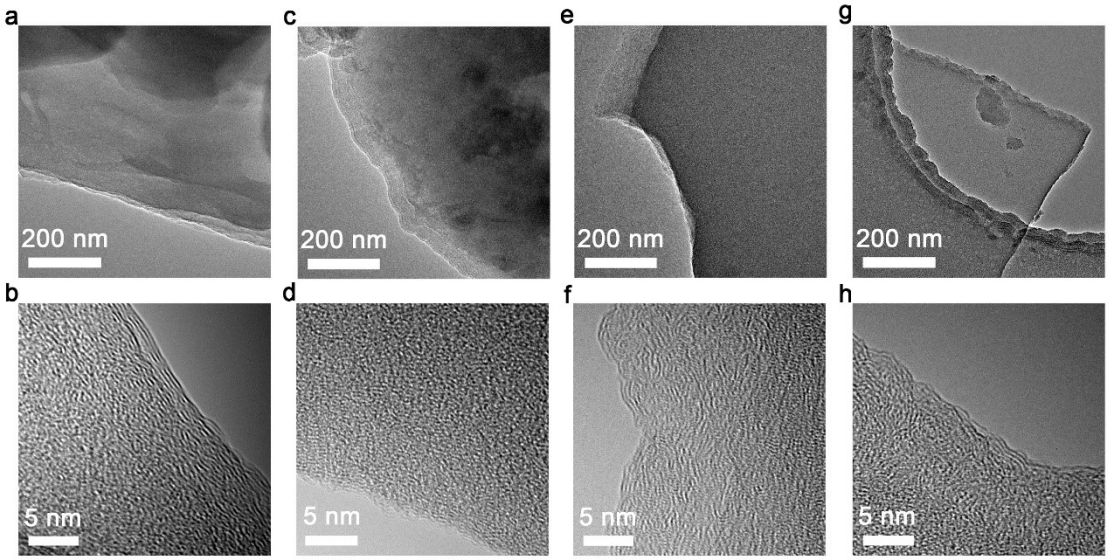

Figure S4. TEM images of catalyst materials prepared with different precursors.(a, b) N-CBMC-500. (c, d) N-XBMC-500. (e, f) N-GBMC-500. (g, h) N-FBMC-500.

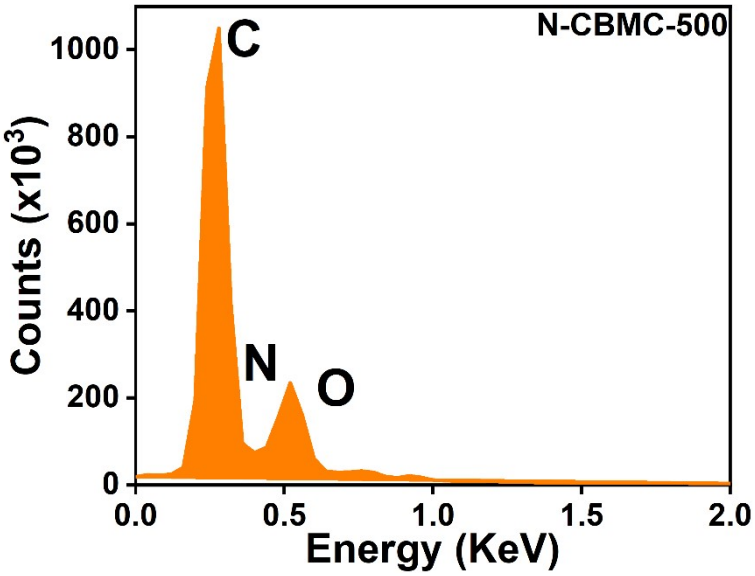

Figure S5. The EDS energy spectrum analysis results of N-CBMC-500.

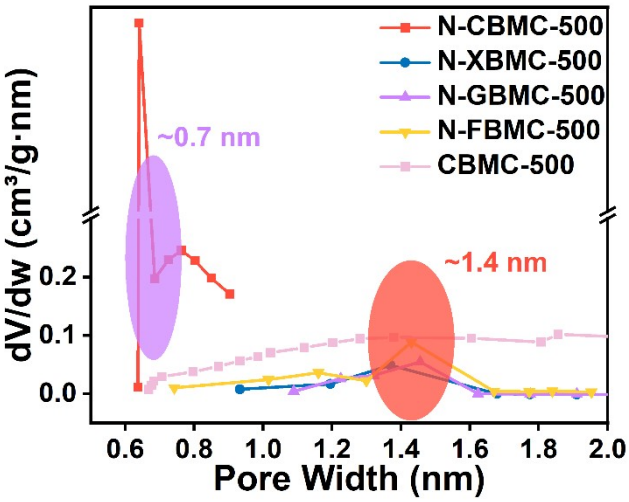

Figure S6. Distribution map of the micropore size of the five catalysts (N-CBMC-500, N-XBMC-500, N-GBMC-500, N-FBMC-500, and CBMC-500).

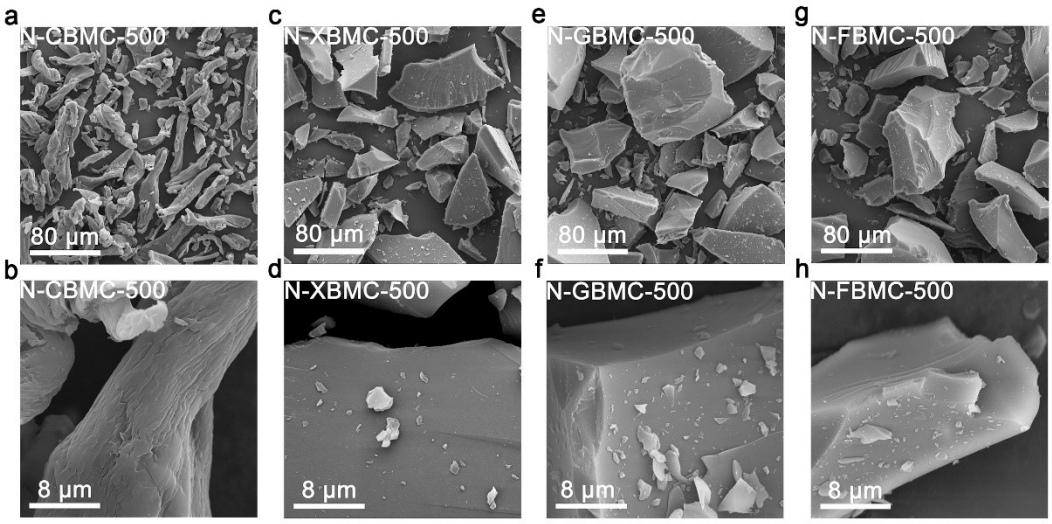

Figure S7. SEM images of catalyst materials prepared with different precursors.(a, b) N-CBMC-500. (c, d) N-XBMC-500. (e, f) N-GBMC-500. (g, h) N-FBMC-500.

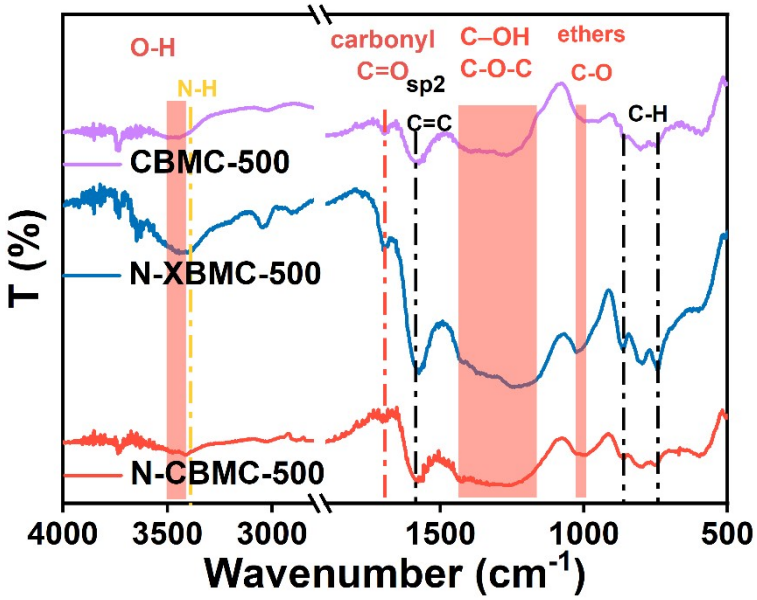

Figure S8. FTIR spectra of N-CBMC-500, N-XBMC-500, and CBMC-500.

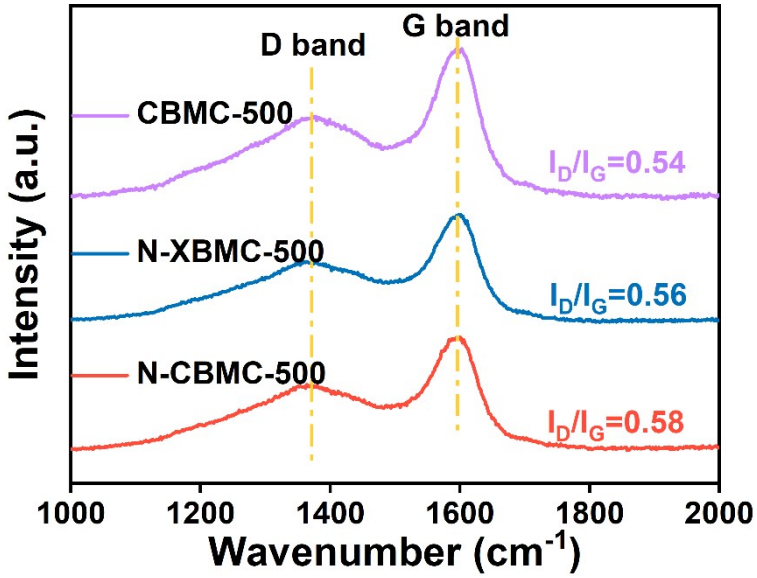

Figure S9. Raman spectra of N-CBMC-500, N-XBMC-500, and CBMC-500.

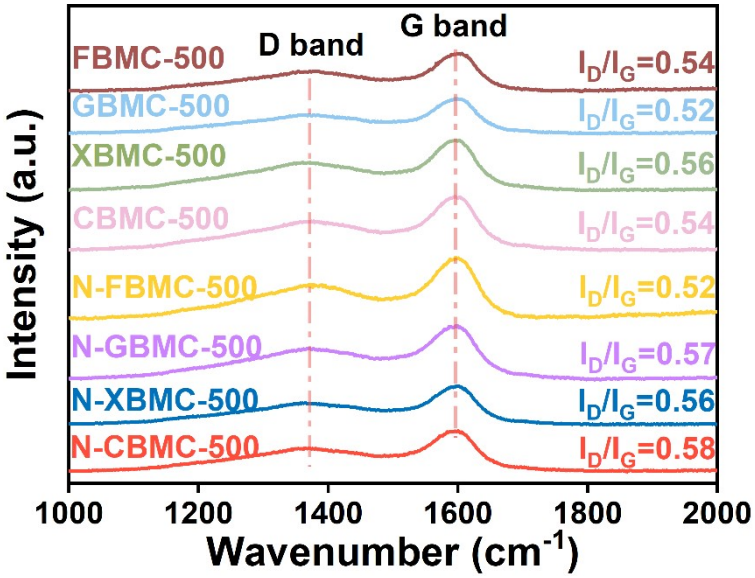

Figure S10. The Raman results of N-doped carbon materials and different precursors carbon materials with no N doping.

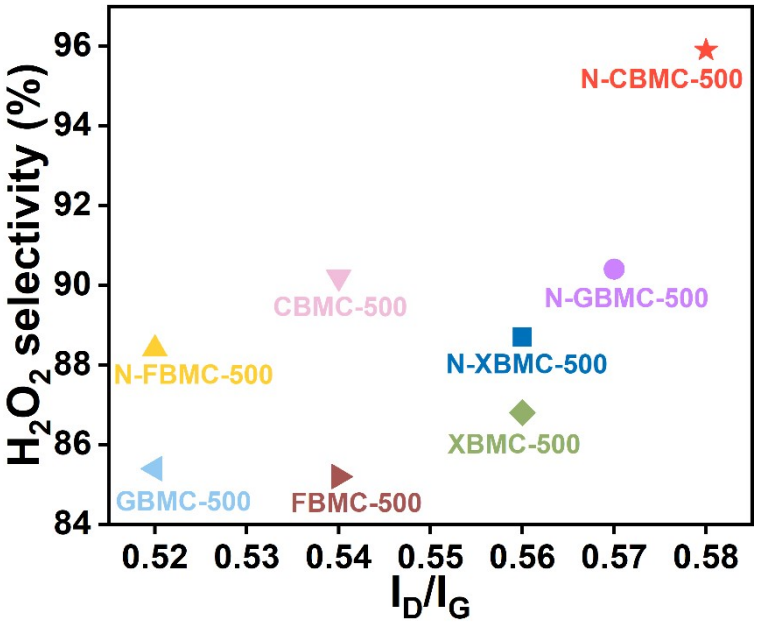

Figure S11. The relationship between I_D/I_G ratio and H_2O_2 selectivity.

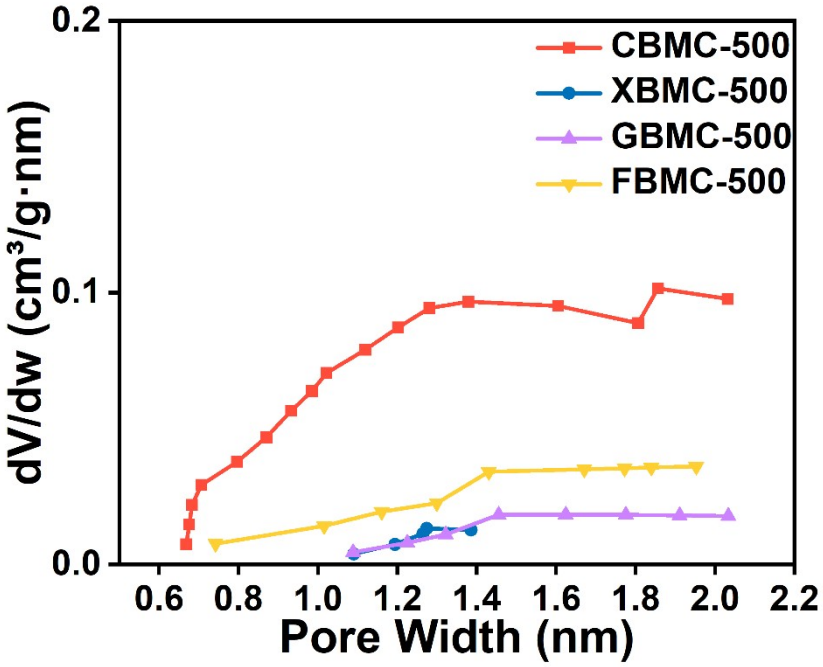

Figure S12. Distribution map of the micropore pore size of the sample without N doping catalysts.

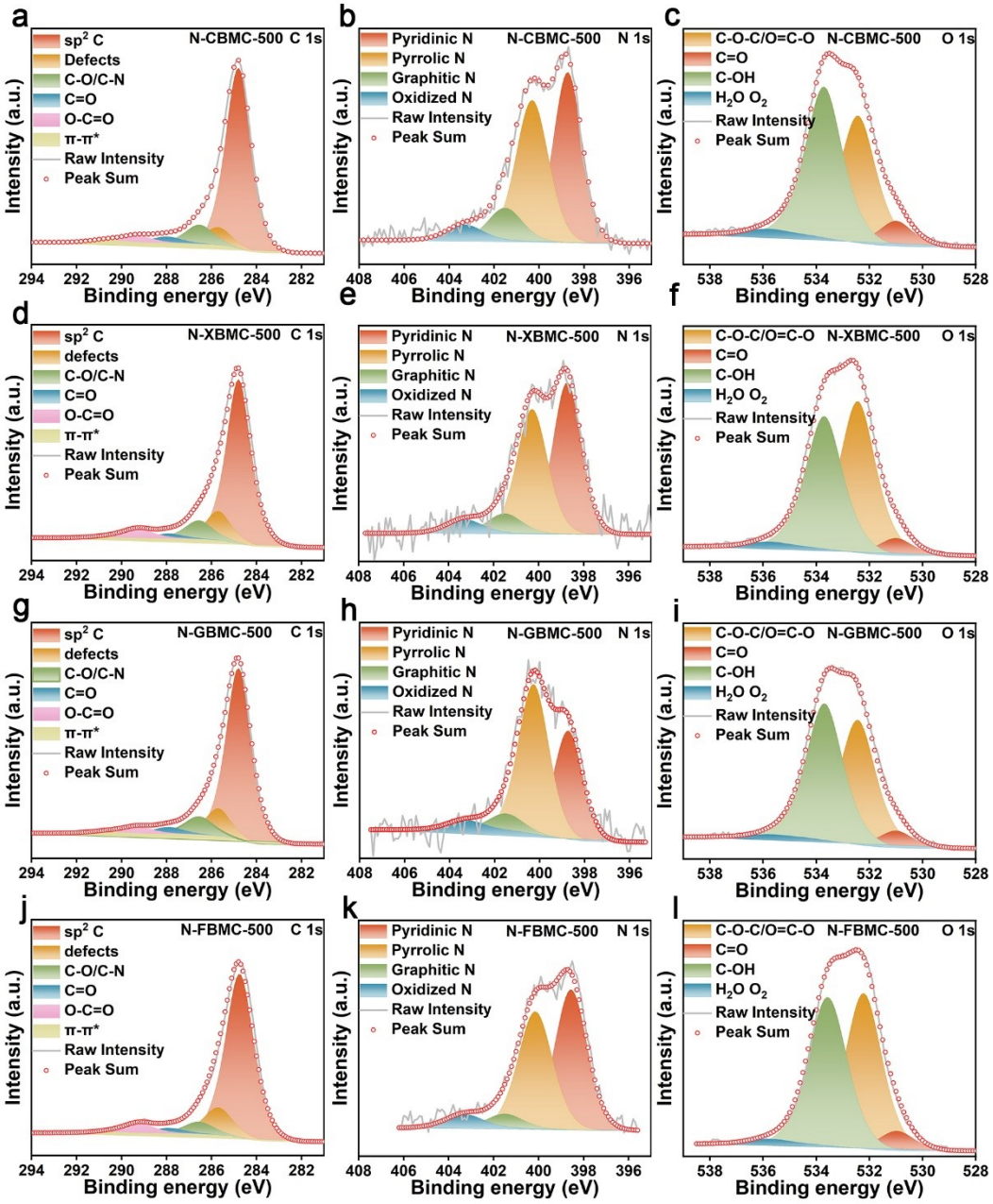

Figure S13. The deconvolution of (a, d, g, j) C 1s, (b, e, h, k) N 1s, and (c, f, i, l) O 1s peaks of N-CBMC-500, N-XBMC-500, N-GBMC-500, and N-FBMC-500

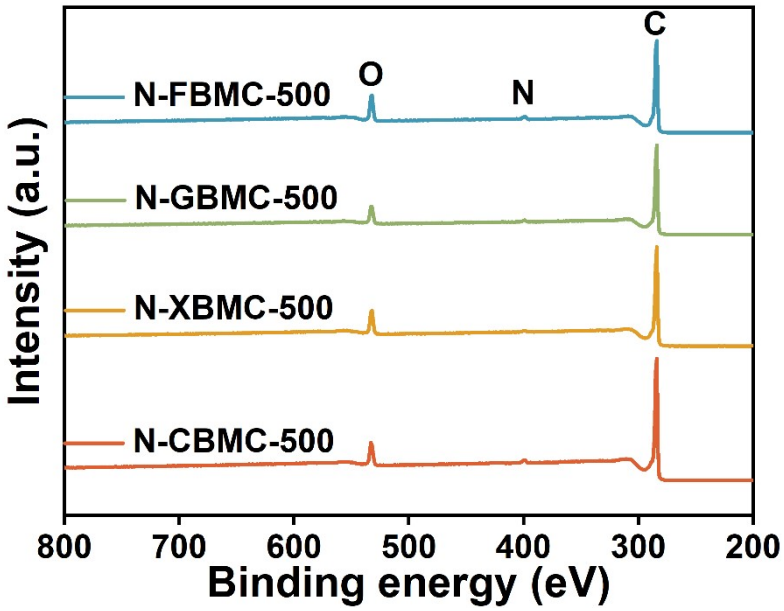

Figure S14. The XPS full survey spectra of four catalysts.

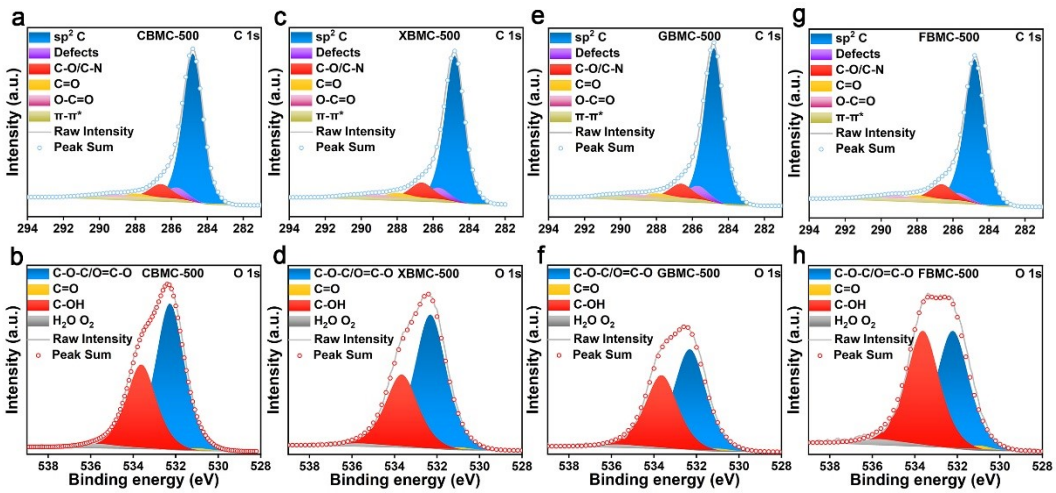

Figure S15. The deconvolution of (a, c, e, g) C 1s and (b, d, f, h) O 1s peaks of CBMC-500, XBMC-500, GBMC-500, and FBMC-500

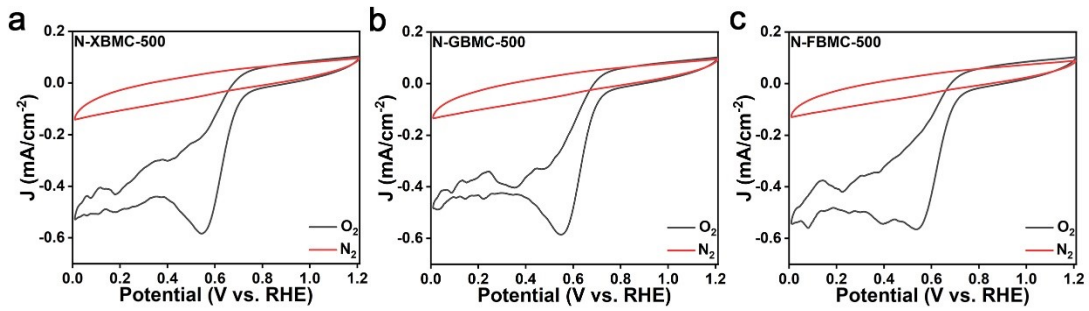

Figure S16. Cyclic voltammograms of N-doped samples in O_2 (solid red line) and N_2 (black dashed line) saturated 0.1 M KOH solution. (a) N-XBMC-500, (b) N-GB,C-500, (c) N-FBMC-500.

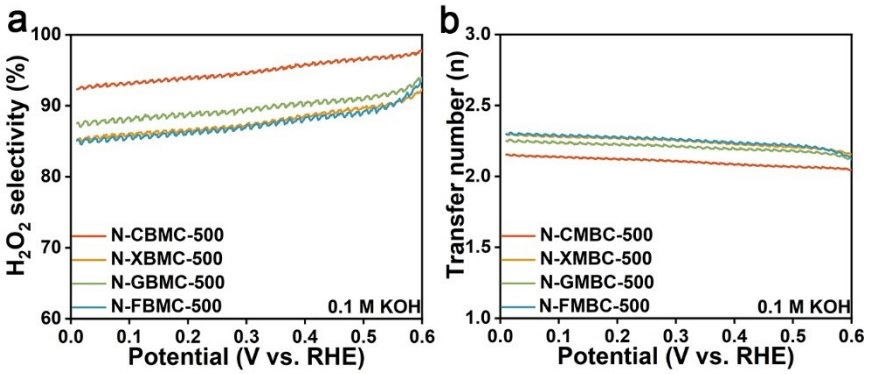

Figure S17. The corresponding (a) H_2O_2 selectivity and (b) electron number of N-CBMC-500, N-XBMC-500, N-GBMC-500, and N-FBMC-500.

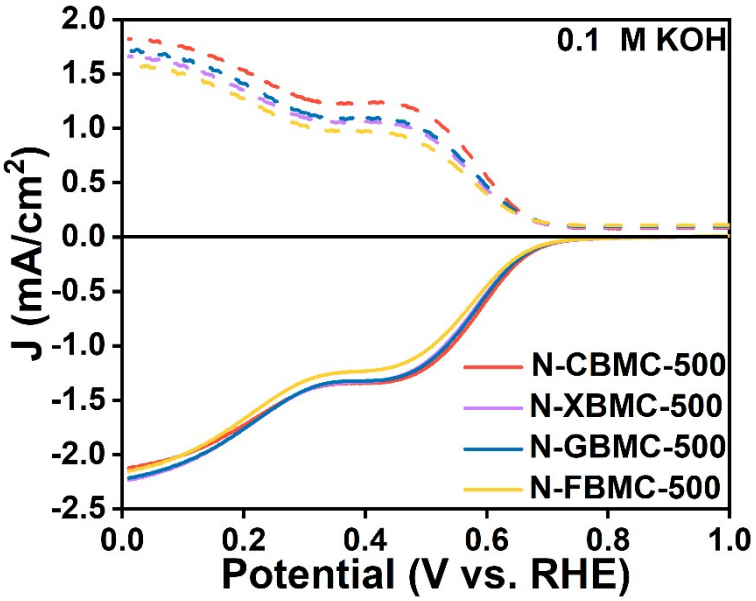

Figure S18. The LSV curves of catalysts prepared with different precursors.

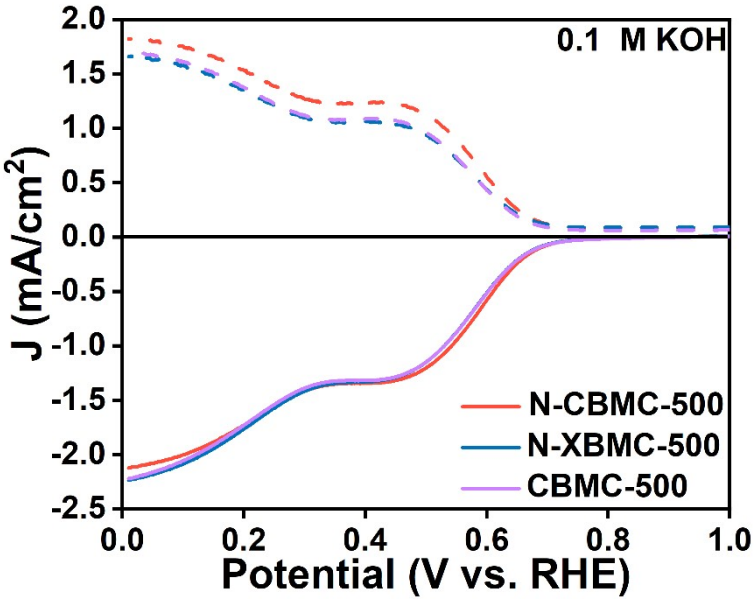

Figure S19. The LSV curves of N-CBMC-500, N-XBMC-500, and CNMC-500 in 0.1 M KOH solution.

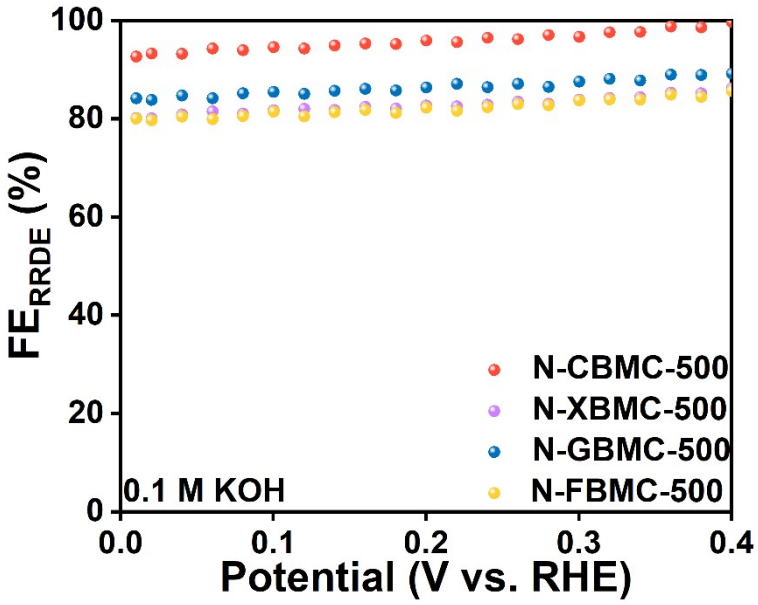

Figure S20. Summary of Faraday efficiency (FE) curve obtained from RRDE test.

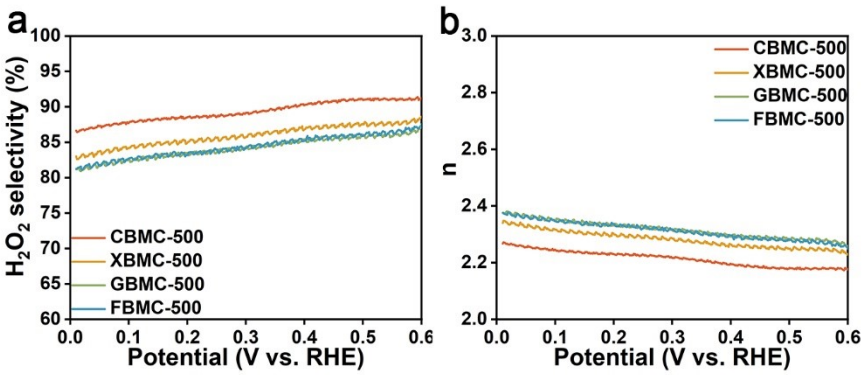

Figure S21. The corresponding (a) H_2O_2 selectivity. and (b) electron number of CBMC-500, XBMC-500, GBMC-500, and FBMC-500.

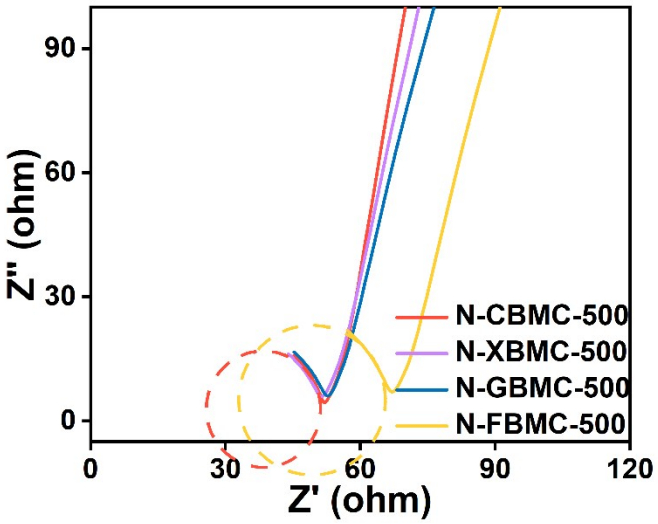

Figure S22. Nyquist plot of EIS for $2e^-$ ORR on N-CBMC-500, N-XBMC-500, N-GBMC-500, and N-FBMC-500 electrodes in 0.1 M KOH at open-circuit voltage.

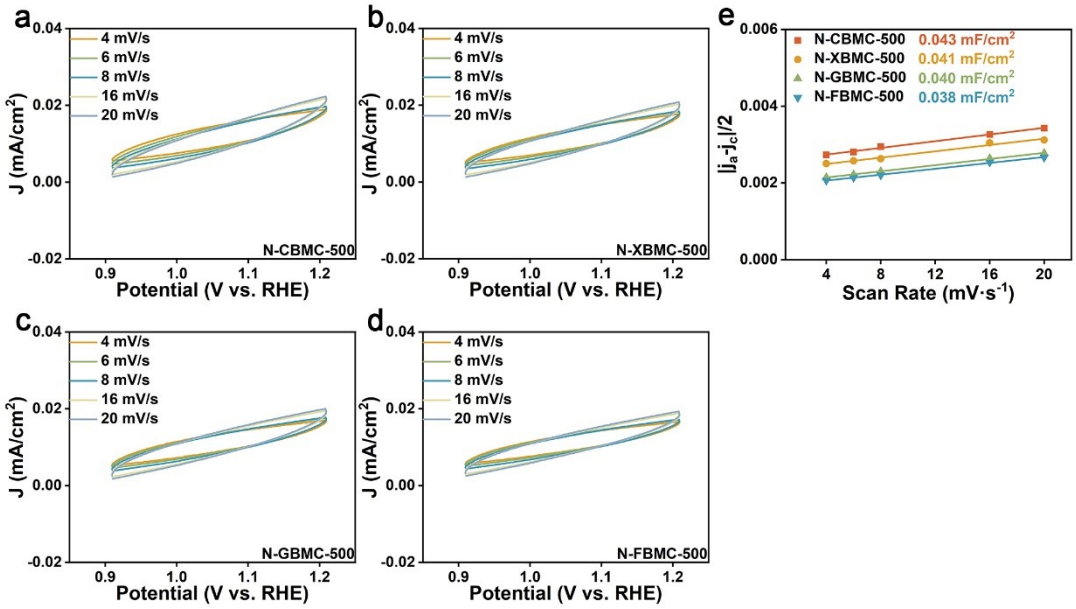

Figure S23. ECSA analysis of N-CBMC-500, N-XBMC-500, N-GBMC-500, and N-FBMC-500. CV curves of (a) N-CBMC-500, (b) N-XBMC-500, (c) N-GBMC-500, and (d) N-FBMC-500 measured in 0.1 M KOH at different scan rates (4, 6, 8, 16, and 20 mV s^{-1}). (E) Half of CV height at 1.05 V (vs. RHE) as a function of scan rate.

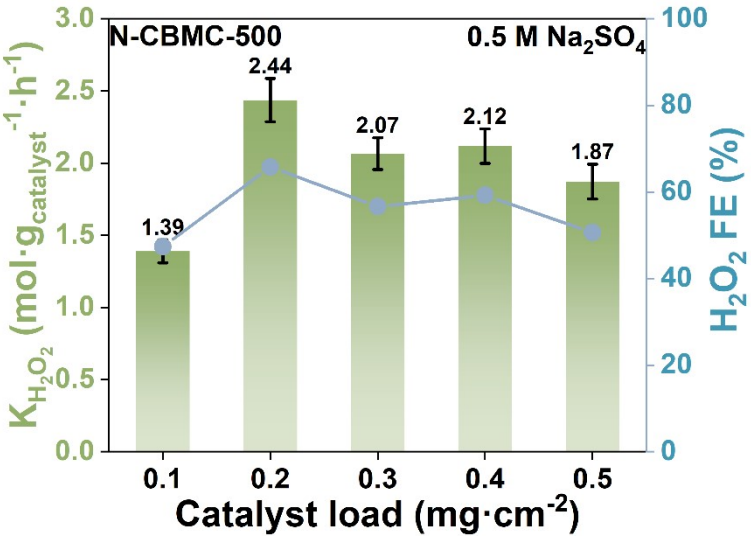

Figure S24. The H_2O_2 yield and FE were measured by chronoamperometry on the N-CBCM-500/GDL with different loadings.

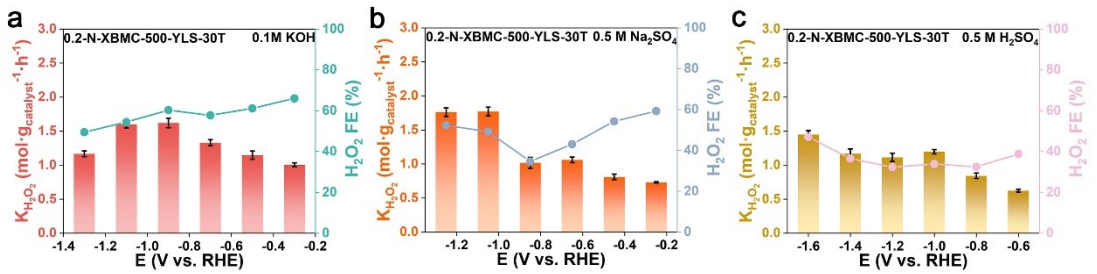

Figure S25. The H_2O_2 yield and FE of N-XBMC-500 in three different pH solutions. (a) 0.1 M KOH, (b) 0.5 M Na_2SO_4, (c) 0.5 M H_2SO_4.

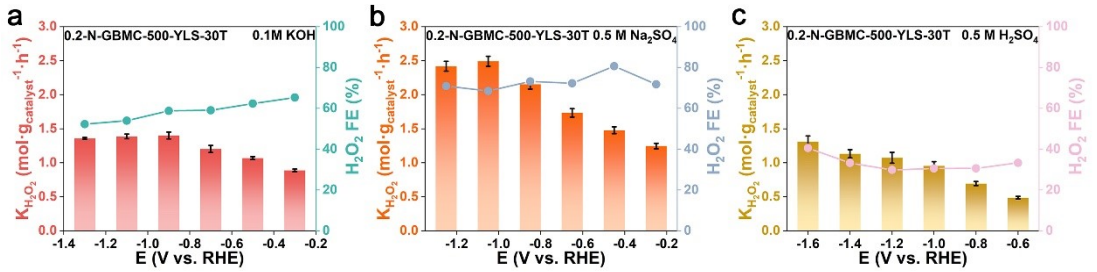

Figure S26. The H_2O_2 yield and FE of N-GBMC-500 in three different pH solutions. (a) 0.1 M KOH, (b) 0.5 M Na_2SO_4, (c) 0.5 M H_2SO_4.

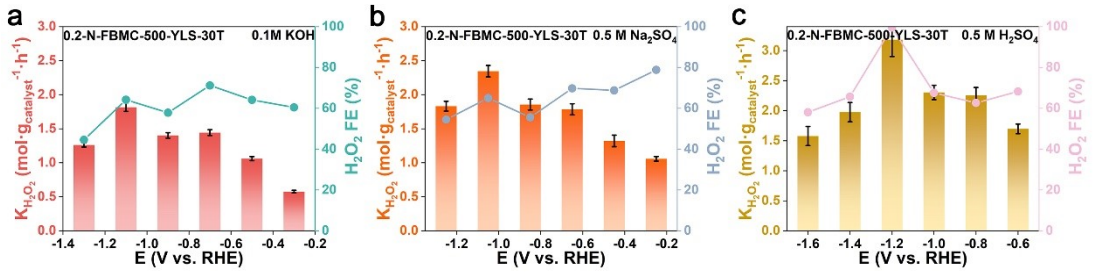

Figure S27. The H_2O_2 yield and FE of N-FBMC-500 in three different pH solutions. (a) 0.1 M KOH, (b) 0.5 M Na_2SO_4, (c) 0.5 M H_2SO_4.

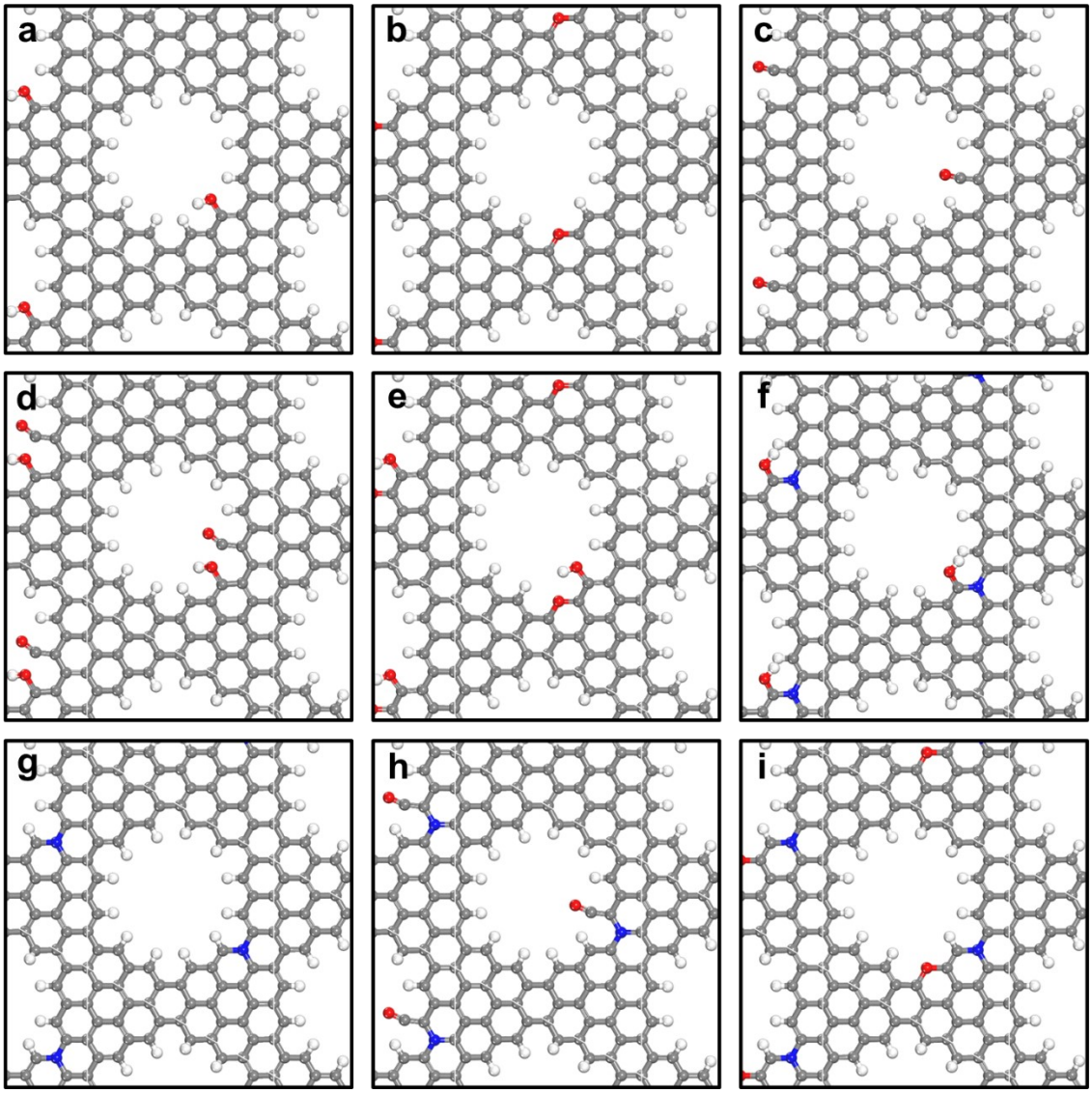

Figure S28. Theoretical analysis of different groups (a) OH; (b) C-O-C; (c) C=O; (d) OH+C=O; (e) OH+C-O-C; (f) OH+N; (g) N; (h) N+C=O; (i) N+C-O-C.

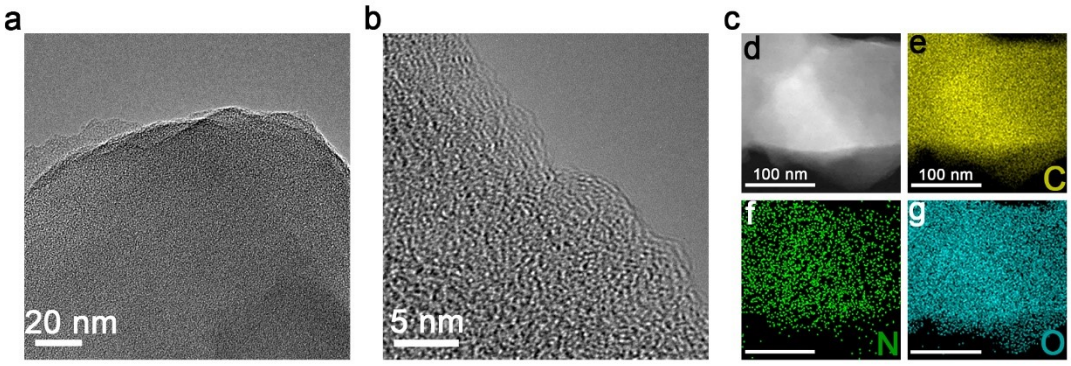

Figure S29. TEM image of N-CBMC-500 after the stability evaluation.

Table S1. Elemental composition of N-CBMC-500, N-XBMC-500, N-GBMC-500, and N-FBMC-500 from EA.

Samples	C (wt%)	H (wt%)	N (wt%)	O (wt%)
N-CBMC-500	85.04	2.99	2.25	9.72
N-XBMC-500	86.55	4.03	1.36	8.06
N-GBMC-500	86.65	4.24	1.12	7.99
N-FBMC-500	85.04	4.32	2.20	8.44

Table S2. Concentrations of carbon species from XPS in N-CBMC-500, N-XBMC-500, N-GBMC-500, and N-FBMC-500.

Samples	sp^2 C=C (at%)	sp^3 C-C (at%)	C-O/C-N(at%)	C=O (at%)	O=C-O (at%)	π-π* (at%)
N-CBMC-500	75.2	7.9	8.8	3.2	3. 5	1.5
N-XBMC-500	69.8	12.9	9.2	2.6	5.1	0.5
N-GBMC-500	68.6	11.2	7.9	7.9	3.3	1.0
N-FBMC-500	73.2	12.7	5.9	2.8	4.8	0.6

Table S3. Concentrations of oxygen species and corresponding binding energy position from XPS in N-CBMC-500, N-XBMC-500, N-GBMC-500, N-FBMC-500, and CBMC-500.

Samples	C=O (at%)	C-O-C O=C-O (at%)	C-OH (at%)	H_2O O_2 (at%)
N-CBMC-500	(531.0 eV) 6.6	(532.4 eV) 41.0	(533.7 eV) 50.3	(535.8 eV) 2.1
N-XBMC-500	(531.0 eV) 5.2	(532.4 eV) 48.8	(533.7 eV) 44.1	(535.8 eV) 1.9
N-GBMC-500	(531.0 eV) 5.6	(532.4 eV) 43.8	(533.7 eV) 49.4	(535.8 eV) 1.2
N-FBMC-500	(531.0 eV) 5.5	(532.2 eV) 46.0	(533.6 eV) 46.7	(535.8 eV) 1.8
CBMC-500	(531.0 eV) 1.1	(532.3 eV) 61.1	(533.6 eV) 36.2	(535.7 eV) 1.6

Table S4. The comparisons between N-CBMC-500 and other metal-free electrocatalysts for H_2O_2 electrochemical synthesis.

Catalysts	pH	Selectivity (RRDE) (%)	H_2O_2 yield				Refs.
			Condition	Production rate		FE (%)	
				mmol h^{-1} g^{-1} RHE	mg L^{-1} h^{-1} RHE		
CDs-2	13	90	/	/	/	/	[13]
MSCH-9:1	8	＞90	/	/	/	/	[14]
2%TBAQ-CNT	7	95	Single Cell V: 300 mL	/	100.4	95	[15]
CB600	7	56.1	Single Cell V: 50 mL floating air cathodes (9.6 cm^2)	/	1035.4	/	[16]
NCA-850	13	~100	H-Cell V: 50-50mL;	/	60	/	[17]
CB-Plasma	13	~100	H-Cell	/	/	100	[18]
O-GOMC-1	13	93	H-Cell Catalyst loading: 0.048 mg cm^{-2}; I=~3 mA	/	51.25	99	[19]
O-GOMC-5.5	13	~90	H-Cell; E=0.6 V(RHE)	/	63.75	99	[20]
$GNP_{C=O,1}$	13	97.8(0.75 V)	H-Cell; E=0.65 V(RHE)	/	6.9	95	[21]
HPC-H24	1 4 7	80.9(0.5 V) ~90(0.5 V) 85.1(0.5 V)	H-Cell Catalyst loading: 0.6 mg cm^{-2}; V: 20-20mL; E=-0.1~-0.5 V(SCE)	294 / 58.3	2249.4(0 V) / 446.8(0.3 V)	91.2 / 60	[22]
N-GO	13	82	H-Cell E=0.2 V(RHE)	224.8	/	43.6	[23]
AGF1100	1 7 13	60	H-Cell V: 30-30mL;	/	472.9(-0.4V) 343(-0.05V) 385.2(0.3V)	68 75.3 72.3	[24]
O-CNT	13	~90	Reactor Catalyst loading: ~2 mg cm^{-2}; V: 25-25mL; E~1.6 V; 46 mA	1161.8	/	/	[25]
CMK-3	13	>90	Reactor Catalyst loading: 0.85 mg cm^{-2}; E~1.6 V	/	1397.5	/	[26]
HCNFs	13	97.3(0.6 V)	Flow-Cell	/	216.6	/	[27]

			Catalyst loading: 0.05 mg cm^{-2};				
$OCNS_{800}$	13	91(0.7 V)	Flow-Cell Catalyst loading: 1.0 mg cm^{-2}; V: 100-100mL; I=50 mA	7.7	178	89.6	[28]
N-CBMC-500	1 7 13	/ / 95.9(0.4V)	Flow-Cell Catalyst loading: 0.2 mg cm^{-2}; V: 100-100mL; E=-1.6~-0.25 V(RHE)	1200(-1.2V) 2460(-0.65V) 2110(-0.9V)	733 1503 1290	34.3 70.0 59.5	**This work**

SUPPORTING REFERENCES

1 U. A. Paulus, T. J. Schmidt, H. A. Gasteiger and R. J. Behm, *J. Electroanal. Chem.*, 2001, **495**, 134-145.

2 Z. Pei, J. Gu, Y. Wang, Z. Tang, Z. Liu, Y. Huang, Y. Huang, J. Zhao, Z. Chen and C. Zhi, *ACS Nano*, 2017, **11**, 6004-6014.

3 C. Xia, J. Y. Kim and H. Wang, *Nat. Catal.*, 2020, **3**, 605-607.

4 R. M. Sellers, *Analyst*, 1980, **105**, 950-954.

5 H. Sheng, E. D. Hermes, X. Yang, D. Ying, A. N. Janes, W. Li, J. R. Schmidt and S. Jin, *ACS Catal.*, 2019, **9**, 8433-8442.

6 J. P. Perdew, K. Burke and M. Ernzerhof, *Phys. Rev. Lett.*, 1996, **77**, 3865-3868.

7 G. Kresse and J. Furthmüller, *Comput. Mater. Sci.*, 1996, **6**, 15-50.

8 G. Kresse and J. Hafner, *Phys. Rev. B*, 1994, **49**, 14251-14269.

9 Z. Yao, C. Guo, Y. Mao and P. Hu, *ACS Catal.*, 2019, **9**, 5957-5973.

10 Z. Wei, Z. Yao, Q. Zhou, G. Zhuang, X. Zhong, S. Deng, X. Li and J. Wang, *ACS Catal.*, 2019, **9**, 10656-10667.

11 Z. Yao, J. Zhao, R. J. Bunting, C. Zhao, P. Hu and J. Wang, *ACS Catal.*, 2021, **11**, 1202-1221.

12 H. J. Monkhorst and J. D. Pack, *Phys. Rev. B*, 1976, **13**, 5188-5192.

13 T.-N. Pham-Truong, T. Petenzi, C. Ranjan, H. Randriamahazaka and J. Ghilane, *Carbon*, 2018, **130**, 544-552.

14 Y. Pang, K. Wang, H. Xie, Y. Sun, M.-M. Titirici and G.-L. Chai, *ACS Catal.*, 2020, **10**, 7434-7442.

15 X. Lu, M. Zhou, Y. Li, P. Su, J. Cai and Y. Pan, *Electrochim. Acta*, 2019, **320**, 134552.

16 H. Zhang, Y. Li, Y. Zhao, G. Li and F. Zhang, *ACS Appl. Mater. Interfaces*, 2019, **11**, 27846-27853.

17 H. Zhao, X. Shen, Y. Chen, S.-N. Zhang, P. Gao, X. Zhen, X. H. Li and G. Zhao, *Chem. Commun.*, 2019, **55**, 6173-6176.

18 Z. Wang, Q.-K. Li, C. Zhang, Z. Cheng, W. Chen, E. A. McHugh, R. A. Carter, B.

I. Yakobson and J. M. Tour, *ACS Catal.*, 2021, **11**, 2454-2459.

19 Y. J. Sa, J. H. Kim and S. H. Joo, *Angew. Chem.*, 2019, **131**, 1112-1117.

20 J. S. Lim, J. H. Kim, J. Woo, D. S. Baek, K. Ihm, T. J. Shin, Y. J. Sa and S. H. Joo, *Chem*, 2021, DOI: https://doi.org/10.1016/j.chempr.2021.08.007.

21 G. F. Han, F. Li, W. Zou, M. Karamad, J. P. Jeon, S. W. Kim, S. J. Kim, Y. Bu, Z. Fu, Y. Lu, S. Siahrostami and J. B. Baek, *Nat. Commun.*, 2020, **11**, 2209.

22 Y. Liu, X. Quan, X. Fan, H. Wang and S. Chen, *Angew. Chem.*, 2015, **127**, 6941-6945.

23 L. Han, Y. Sun, S. Li, C. Cheng, C. E. Halbig, P. Feicht, J. L. Hübner, P. Strasser and S. Eigler, *ACS Catal.*, 2019, **9**, 1283-1288.

24 Z. Pan, K. Wang, Y. Wang, P. Tsiakaras and S. Song, *Applied Catalysis B: Environmental*, 2018, **237**, 392-400.

25 H. W. Kim, M. B. Ross, N. Kornienko, L. Zhang, J. Guo, P. Yang and B. D. McCloskey, *Nat. Catal.*, 2018, **1**, 282-290.

26 Z. Chen, S. Chen, S. Siahrostami, P. Chakthranont, C. Hahn, D. Nordlund, S. Dimosthenis, J. K. Nørskov, Z. Bao and T. F. Jaramillo, *Reaction Chemistry & Engineering*, 2017, **2**, 239-245.

27 K. Dong, J. Liang, Y. Wang, Z. Xu, Q. Liu, Y. Luo, T. Li, L. Li, X. Shi, A. M. Asiri, Q. Li, D. Ma and X. Sun, *Angew. Chem., Int. Ed.*, 2021, **60**, 10583-10587.

28 S. Chen, T. Luo, K. Chen, Y. Lin, J. Fu, K. Liu, C. Cai, Q. Wang, H. Li, X. Li, J. Hu, H. Li, M. Zhu and M. Liu, *Angew. Chem., Int. Ed.*, 2021, **60**, 16607-16614.